Chinese Chemical Letters 35 (2024) 109401

Contents lists available at ScienceDirect

Chinese Chemical Letters

journal homepage: www.elsevier.com/locate/cclet

Single droplet formation by controlling the viscoelasticity of polymer solutions during inkjet printing

Dong Lv[a,b], Xuelei Liu[a,b], Wei Li[a,b], Qiang Zhang[a], Xinhong Yu[a,*], Yanchun Han[a,b,*]

[a] State Key Laboratory of Polymer Physics and Chemistry, Changchun Institute of Applied Chemistry, Chinese Academy of Sciences, Changchun 130022, China
[b] School of Applied Chemistry and Engineering, University of Science and Technology of China, Hefei 230026, China

ARTICLE INFO

Article history:
Received 14 November 2023
Revised 14 December 2023
Accepted 15 December 2023
Available online 19 December 2023

Keywords:
Inkjet printing
Single droplet
Satellite droplet
Viscoelasticity
Coil-stretch

ABSTRACT

Inkjet printing has emerged as a potential solution processing method for large-area patterned films. During inkjet printing, a single droplet without satellite droplet is required for high-quality film. Herein, we propose a strategy for obtaining a single droplet by adjusting the reduced concentration (c/c^*, where c^* is the critical overlap concentration) in the range of 1.0–1.5. Droplet formation can be categorized into three distinct regimes: (1) $c/c^* < 1.0$, satellite droplet; (2) $c/c^* = 1.0–1.5$, single droplet; (3) $c/c^* > 2.0$, no droplet. Furthermore, an inertial-capillary balance led to the 2/3-power scaling of the minimum radius with time for the solutions of $c/c^* < 1.0$. However, for the solutions of $c/c^* = 1.0–1.5$, the ligament radius decreased exponentially with time. Moreover, the Weissenberg number was higher than the critical value of 0.5, indicating that the polymer chains underwent coil-stretch transition. The viscoelastic-capillary balance dominated instead of the inertial-capillary balance. The resulting viscoelastic resistance reduced the length of the ligament and increased the velocity difference between the satellite and main droplets. Consequently, a single droplet was formed. In addition, the law can be successfully generalized to various molecular weights, molecular structures and solvents.

Inkjet printing technology is considered as a highly promising solution processing method for film formation, due to its wide range of applicable materials and high material utilization [1–3]. One of the key challenges is the formation of single droplets with the suitable velocity, volume and excellent reliability [4,5]. This is particularly critical, as satellite droplets during inkjet printing can have a significant impact on the quality of the resulting film, such as inducing incorrect stains, asymmetrical coalescence of droplets on the substrate, and deviating from the predetermined printing position [6–8]. The formation of droplets is an intricate process that is governed by the complex interplay of capillary, inertial, viscous, and elastic effects [9,10]. As for a drop-on-demand (DOD) inkjet printer, the piezoelectric transducer deforms by applying voltage signals to squeeze the solutions from nozzle to form ligament. According to the Young-Laplace equation, the capillary pressure is proportional to the curvature of interface, and the pinch-off commonly occurs at the position with the greatest curvature variation, that is, the corresponding largest pressure gradient [11,12]. Newtonian fluid solutions (comprised of pure solvents and small molecular solutions) exhibit a predictable and concise droplet formation that is primarily governed by physical parameters such as viscosity and surface tension [13,14]. However, for polymer solutions, other important physical parameters also must be taken into account, with viscoelasticity being a particularly crucial parameter. The incorporation of small amounts of polymer into the ink composition results in a significantly more complex fluid system, and the resultant viscoelasticity can significantly impact the pinch-off and detachment dynamics of droplets during the printing process [11,15–18]. In order to better understand this phenomenon, a dripping-onto-substrate rheometer was employed to simulate the process of ligament thinning. The results indicated that the ligament thinning process of Newtonian fluids was governed by either an inertio-capillary (IC) or a visco-capillary (VC) balance, until the eventual breakup of the ligament. However, as the radius of the ligament decreased, the ligament thinning process of polymer solutions underwent elasto-capillary (EC) thinning stage. The viscoelastic stress generated by polymer stretching masked the inertial effect and emerged as the dominant stress component, thereby increasing both the pinch-off time and length [9,19]. The conformation transition from coil to stretch state of polymer chains has

* Corresponding authors.
E-mail addresses: xhyu@ciac.ac.cn (X. Yu), ychan@ciac.ac.cn (Y. Han).

https://doi.org/10.1016/j.cclet.2023.109401
1001-8417/

been demonstrated to occur under the inkjet printing process [20]. The Weissenberg number (*Wi*) was a criterion for determining the occurrence of the coil-stretch transition (Eq. 1) [16,21].

$$Wi = \varepsilon \cdot \lambda \tag{1}$$

where ε is the elongation rate, and λ is the relaxation time. When *Wi* was less than 0.5, the polymer chains relaxed and the solution behaved like Newtonian fluid. Conversely, when *Wi* surpassed 0.5, the polymer chains began to undergo the coil-stretch transition, and the solution exhibited viscoelasticity [10,18,22]. According to the Zimm model, the relaxation time in an infinitely dilute polymer solution can be described through the following expression (Eq. 2):

$$\lambda_{\text{Zimm}} = \frac{\eta_s[\eta]M_w}{RT} \tag{2}$$

where η_s is the viscosity of the solvent, $[\eta]$ is the intrinsic viscosity, M_w is the molecular weight, R is the gas constant, and T is the temperature. Based on the expression of the relaxation time as depicted in Eq. 2, it can be deduced that concentration, molecular weight, molecular structure and solvent are the essential factors determining the relaxation time. To account for the interplay of all relevant parameters, the critical overlap concentration, c^*, is introduced, which is related to molecular weight, molecular structure of polymer and solvent. The measurement and calculation of c^* are shown in Eqs. S1-S4 and Fig. S3 (Supporting information). Subsequently, the reduced concentration (c/c^*) were used instead of the commonly used concentrations to explore the droplet formation process.

In this work, a charge-coupled device (CCD) camera was employed to observe and record the droplet formation process. As illustrated in Fig. 1, under the same reduced concentration, the droplet formation remained almost identical, irrespective of variations in molecular weights, molecular structures, and solvents. For $c/c^* = 0.3$ and 0.5, the main droplet and satellite droplet were formed due to the head pinch-off of ligament. Two droplets were ultimately formed. When the reduced concentration exceeded 1.0, a single droplet was formed due to the mergence of the main droplet and satellite droplet. Beyond $c/c^* = 2.5$, no droplet was formed due to insufficient kinetic energy to overcome the resistance, thereby preventing the ligament from detaching and returning to the nozzle. Moreover, as shown in Figs. S5 and S6 (Supporting information), the extracted trajectory data of droplets revealed that the velocity of droplets formed by solutions at concentrations of $c/c^* = 1.0$ and 1.5 was 1.40 and 1.09 m/s respectively, while the velocity of droplet formed by the solution at $c/c^* = 2.0$ was 0.83 m/s, which was below the minimum velocity of 1.00 m/s required for inkjet printing [23,24]. Thus, the concentration range for forming a single droplet was $c/c^* = 1.0$–1.5 for all solutions with various molecular weights, molecular structures and solvents.

To explore the significant changes in droplet formation in solutions with the reduced concentrations ranging from 0.5 to 1.0, the ligament diameter was analyzed at the tail pinch-off (near the nozzle) and head pinch-off locations (near the main droplet). Previous studies have indicated that in situations characterized by low viscosity and inelasticity, the evolution of the diameter can be described as an inertia-capillary thinning response [25,26].

The relationship between the relative diameter and time in such cases is known to follow a 2/3 power law (Eq. 3) [27,28].

$$\frac{D_m(t)}{D_0} = X\left(\frac{t_c - t}{t_R}\right)^{2/3} \tag{3}$$

here, D_0 is the initial diameter of the ligament, t_c is the pinch-off time, X is the prefactor, and t_R is the Rayleigh time, which depends on the material properties of the fluid (density and surface tension) and the characteristic length scale. However, when the concentration increases to the point where elasticity begins to have a significant impact, the thinning process of the ligament is controlled by the balance between capillary force and elastic force. In these conditions, the evolution of the ligament diameter follows an exponential law (Eq. 4) [19,29–32].

$$\frac{D_m(t)}{D_0} \approx \left(\frac{G_E R_0}{2\sigma}\right)^{1/3} \exp\left(\frac{t_c - t}{3\lambda_e}\right) \tag{4}$$

where G_E is the extensional elastic modulus, R_0 is the initial radius, σ is the surface tension and λ_e is relaxation time.

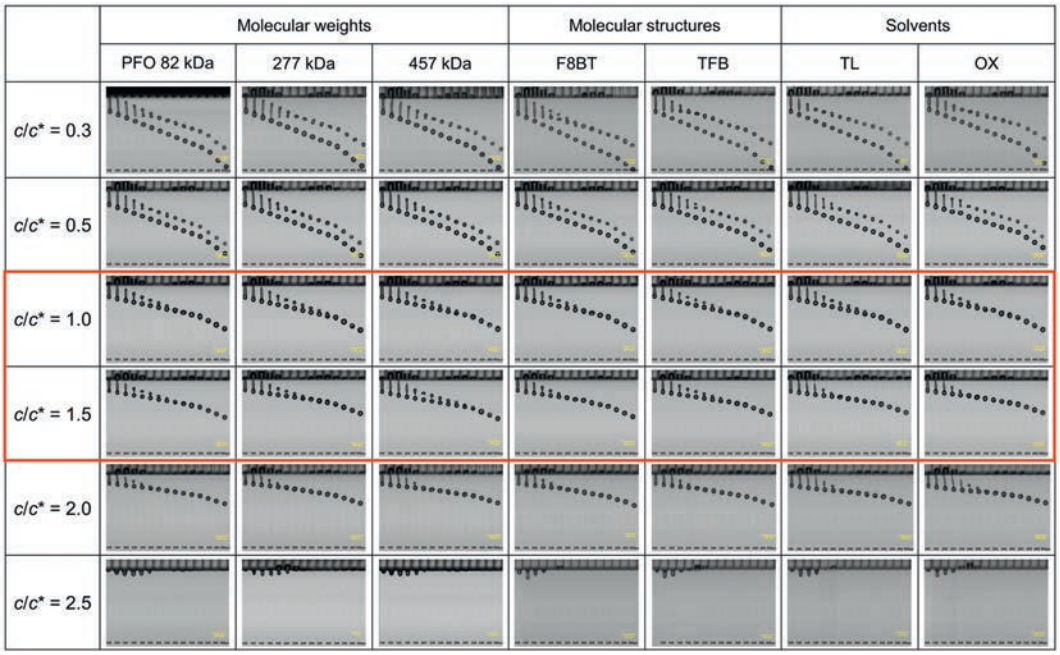

Fig. 1. Representative photo sequence of the droplets as a function of the elapsed time for the solutions with different molecular weights, molecular structures and solvents at different reduced concentrations ($c/c^* = 0.3$, 0.5, 1.0, 1.5, 2.0, 2.5). Scale bar: 200 μm.

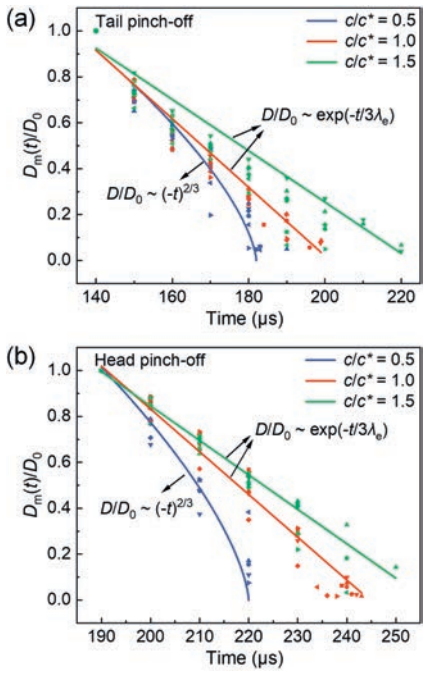

Fig. 2. Relationship between the normalized ligament diameter of solutions ($c/c^* = 0.5$, 1.0 and 1.5) and time. (a) Tail pinch-off. (b) Head pinch-off.

As depicted in Fig. 2a, the evolution of the normalized ligament diameter at the tail pinch-off location for the solutions at $c/c^* = 0.5$ adhered to the 2/3 power law, while that of the solutions at $c/c^* = 1.0$ and 1.5 conformed to the exponential law. The confidence levels of the fitted curves were greater than 95%. A similar pattern was observed at the head pinch-off location, as illustrated in Fig. 2b. This indicates that viscoelastic force was present at both pinch-off locations in the solutions at $c/c^* = 1.0$ and 1.5, whereas it was opposite for the solutions at $c/c^* = 0.5$. According to Eq. 4, the effective relaxation time can be derived from the fitting relationship of ligament diameter evolution. For the convenience of calculation, the natural logarithm was applied on both sides of the equation, as represented in Eq. 5.

$$\ln\left[\frac{D_m(t)}{D_0}\right] = \frac{1}{3\lambda_e}(t_c - t) + \frac{1}{3}\ln\left(\frac{G_E R_0}{2\sigma}\right) \quad (5)$$

In Figs. 3a and b, a good linear fit of $\ln[(D_m(t)/D_0]$ as a function of $(t_c\text{-}t)$ can be obtained for all the solutions. This allowed the reliable calculation of the effective relaxation time $\lambda_e = 1/(3k)$ (k is the slope). The effective relaxation time of solutions with different reduced concentrations were listed in Table S7 (Supporting information). For the solutions at $c/c^* = 1.0$, the effective relaxation time at the tail and head pinch-off were 10.32 ± 0.58 μs and 10.54 ± 0.19 μs, respectively. For the solutions at $c/c^* = 1.5$, these values were 13.56 ± 0.29 μs and 14.72 ± 0.35 μs.

The elongation rate (ε) at pinch-off time t_c can be estimated from the decrease of ligament diameter between t_c and the time t near the pinch-off time (Eq. 6) [29].

$$\varepsilon = -\frac{2}{D_m}\frac{dD_m}{dt} \approx \frac{2}{D_t}\frac{D_t - D_c}{t_c - t} \quad (6)$$

The Weissenberg number (Wi) was the product of effective relaxation time and the elongation rate (Eq. 1), as shown in Figs. 3c and d, and Table S7. The Wi was determined to be 2.71 ± 0.08 at tail pinch-off and 2.86 ± 0.10 at head pinch-off for the solutions at the concentration of $c/c^* = 1.0$. For $c/c^* = 1.5$, the Wi was greater, which was 3.72 ± 0.06 at tail pinch-off and 3.91 ± 0.09 at head pinch-off. These values were greater than the critical value of 0.5, indicating that the polymer chains underwent coil-stretch transition at the tail and head pinch-off locations.

The viscoelasticity generated by the coil-stretch transition of polymer chains has a substantial impact on the formation of lig-

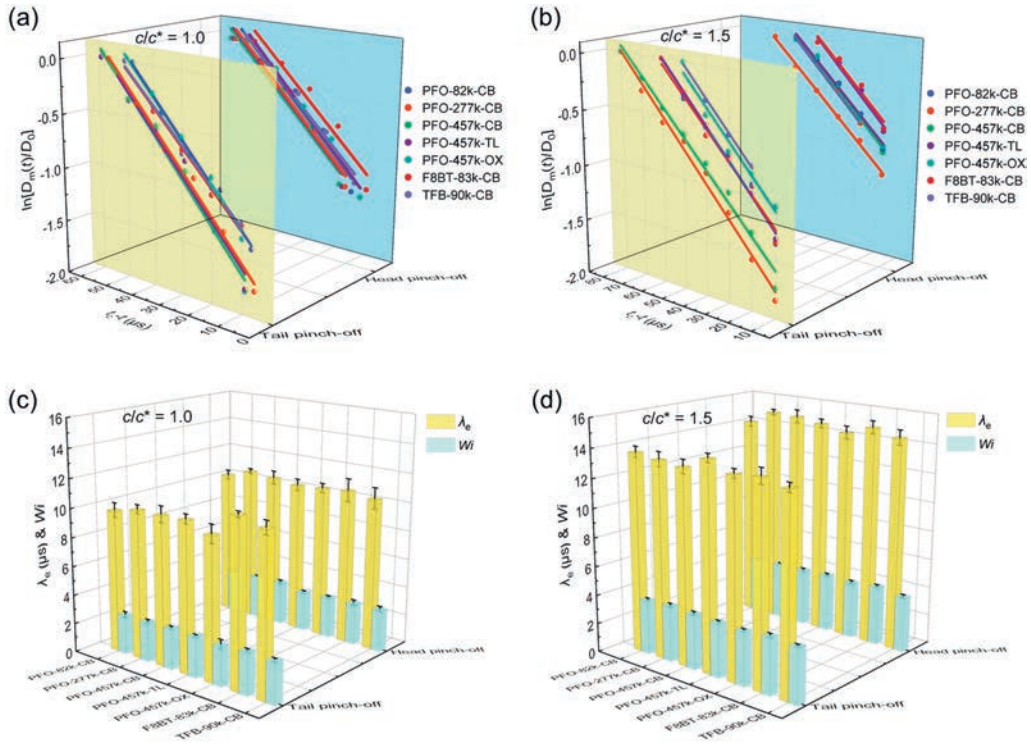

Fig. 3. The logarithmic normalized ligament diameter as function of the logarithmic shifted time ($t_c\text{-}t$) at tail and head pinch-off time. (a) $c/c^* = 1.0$. (b) $c/c^* = 1.5$. The effective relaxation time (λ_e) and calculated Wi at tail and head pinch-off time. (c) $c/c^* = 1.0$. (d) $c/c^* = 1.5$.

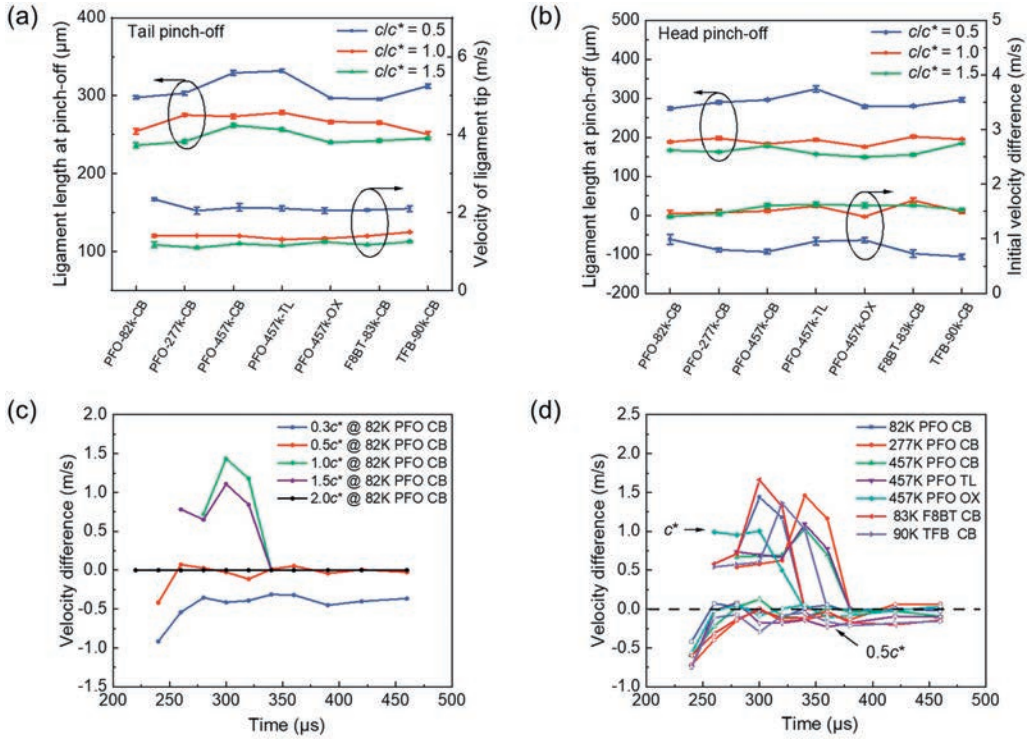

Fig. 4. (a) The ligament length and velocity at the tail pinch-off time of solutions at $c/c^* = 0.5$, 1.0 and 1.5. (b) The ligament length when head pinch-off occurred and initial velocity difference of main and satellite droplets. (c) The velocity difference between satellite and main droplets for the solutions dissolving 82 kDa PFO in CB/CHB = 80/20 solvent at different reduced concentrations ($c/c^* = 0.3$, 0.5, 1.0, 1.5, 2.0). (d) The velocity difference of all solutions at $c/c^* = 0.5$ and 1.0 with different molecular weights, solvents and molecular structures used in the experiment.

ament and droplet. Whether the droplets merge or not was mainly determined by the distance and velocity of the main and satellite droplets. As shown in Fig. 4a, as the reduced concentration rose, the ligament length at the moment of tail pinch-off gradually decreased, while the velocity at the tip of ligament also decreased. These were beneficial for droplet mergence. After the ligament was disconnected from the nozzle, the droplet had no additional force and was in a state of free flight. The stretched polymer chains in the ligament intensified the traction of the head and tail of the ligament towards each other. As a result, the ligament length of head pinch-off gradually decreased as the concentration increased. The velocity difference was defined as the difference in velocity between the satellite droplet and main droplet. The initial velocity difference increased with concentration (Fig. 4b). These also facilitated the mergence of the two droplets. Subsequently, the association between the velocity difference and time was plotted using 82 kDa PFO CB inks as an example (Fig. 4c). The velocity difference consistently stayed below zero at the reduced concentration of 0.3. This demonstrated that the satellite and main droplet finally became too far apart to mix into a single droplet when the distance between them grew over time. The velocity difference fluctuated between positive and negative values for $c/c^* = 0.5$. The satellite droplet did not catch up to the main droplet as the main droplet was 291 ± 17 μm ahead of it at head pinch-off. Consequently, two droplets were formed. The velocity difference constantly exceeded zero when $c/c^* \geq 1.0$, demonstrating that the satellite droplet was able to close the distance gap between it and the main droplet. The same trend was obtained for other solutions, regardless of variations in molecular weight, solvent and molecular structure, as shown in Fig. 4d. Therefore, the schematic diagram of droplet formation at various reduced concentrations was plotted based on the data mentioned above (Fig. 5). The stretched polymer chains emerged in the ligament of the solutions with the concentration

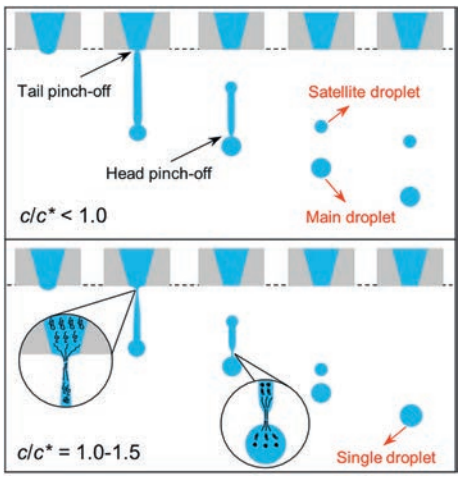

Fig. 5. Schematic illustration of droplet formation for the solutions at $c/c^* < 1.0$ and $c/c^* = 1.0$–1.5.

of $c/c^* = 1.0$–1.5, while they were absent from those with reduced concentration of 0.5. The viscoelastic resistance that resulted from this contributed to the balance of inertial force. As a result, the ligament length shrank and the velocity difference between the satellite and main droplets widened. The interaction of these effects encouraged the mergence of two droplets into a single droplet.

In summary, a single droplet was obtained by adjusting the reduced concentration within the range of $c/c^* = 1.0$–1.5. This law can be generalized to different molecular weights, molecular structures and solvents. The results of minimum radius evolution indicated that the ligament produced by the solutions at $c/c^* = 0.5$ exhibited the typical inertia-capillary interaction. However, when $c/c^* = 1.0$–

1.5, the ligament followed viscoelastic-capillary interaction. Furthermore, the Weissenberg number (*Wi*) was great than 0.5, indicating that the polymer chains underwent coil-stretch transition. The resulting viscoelastic resistance reduced the ligament length and the main droplet velocity. This provided an opportunity for the single droplet formation. Consequently, this work provides a valuable guidance for the formulation of polymer solutions used in inkjet printing.

Declaration of competing interest

The authors declare that they have no known competing financial interests or personal relationships that could have appeared to influence the work reported in this paper.

Acknowledgments

This work was financially supported by the National Natural Science Foundation of China (No. 51873212) and the CAS-Croucher Funding Scheme for Joint Laboratories: PolyU-CIAC Joint Laboratory (No. 121522KYSB20200040).

Supplementary materials

Supplementary material associated with this article can be found, in the online version, at doi:10.1016/j.cclet.2023.109401.

References

[1] B.J. de Gans, P.C. Duineveld, U.S. Schubert, Adv. Mater. 16 (2004) 203–213.
[2] X.H. Cao, Y. Ye, Q. Tang, et al., J. Phys. Chem. Lett. 11 (2020) 8442–8450.
[3] Q. Zhang, J.G. Liu, X.H. Yu, Y.C. Han, Chin. Chem. Lett. 30 (2019) 1405–1409.
[4] B. Derby, Engineering 1 (2015) 113–123.
[5] R.Q. Tao, Z.Q. Fang, J.H. Zhang, et al., ACS Appl. Mater. Interfaces 10 (2018) 22883–22888.
[6] Z.H. Du, R.B. Xing, X.X. Cao, et al., Polymer 115 (2017) 45–51.
[7] J. Hong, Y. Jin, Y. Jin, et al., Langmuir 38 (2022) 15839–15847.
[8] X.H. Yu, R.B. Xing, Z.X. Peng, et al., Chin. Chem. Lett. 30 (2019) 135–138.
[9] J.R. Castrejon-Pita, A.A. Castrejon-Pita, S.S. Thete, et al., Proc. Natl. Acad. Sci. U. S. A. 112 (2015) 4582–4587.
[10] Z.H. Du, Y.M. Lin, R.B. Xing, et al., Polymer 138 (2018) 75–82.
[11] C.X. Xu, Z.Y. Zhang, J.Z. Fu, Y. Huang, Langmuir 33 (2017) 5037–5045.
[12] A. Fraters, R. Jeurissen, M. van den Berg, et al., Phys. Rev. Appl. 13 (2020) 024075.
[13] S. Krainer, C. Smit, U. Hirn, RSC Adv. 9 (2019) 31708–31719.
[14] S.H. Kang, S. Kim, D.K. Sohn, H.S. Ko, Phys. Fluids 32 (2020) 010401.
[15] H.J. Shore, G.M. Harrison, Phys. Fluids 17 (2005) 033104.
[16] Z.H. Du, X.H. Yu, Y.C. Han, Chin. Chem. Lett. 29 (2018) 399–404.
[17] N.F. Morrison, O.G. Harlen, Rheol. Acta 49 (2010) 619–632.
[18] S.D. Hoath, O.G. Harlen, I.M. Hutchings, J. Rheol. 56 (2012) 1109–1127.
[19] J. Dinic, V. Sharma, Proc. Natl. Acad. Sci. U. S. A. 116 (2019) 8766–8774.
[20] R.I. Haque, R. Vié, M. Germainy, et al., Flexible Print. Electron. 1 (2015) 015001.
[21] Z.H. Du, H. Zhou, W.R. Cao, et al., Chin. Chem. Lett. 31 (2020) 3216–3220.
[22] S.D. Hoath, D.C. Vadillo, O.G. Harlen, et al., J. Non-Newton Fluid Mech. 205 (2014) 1–10.
[23] S.D. Hoath, W.K. Hsiao, S.J. Jung, et al., J. Imaging Sci. Technol. 57 (2013) 010503.
[24] Y.E. Wang, X.P. Li, C.C. Li, et al., J. Mater. Sci. 50 (2015) 5014–5023.
[25] J. Dinic, V. Sharma, Macromolecules 53 (2020) 3424–3437.
[26] S. Sur, J. Rothstein, J. Rheol. 62 (2018) 1245–1259.
[27] L.N. Jimenez, J. Dinic, N. Parsi, V. Sharma, Macromolecules 51 (2018) 5191–5208.
[28] J. Dinic, V. Sharma, Macromolecules 53 (2020) 4821–4835.
[29] S.G. Kim, H.S. Lee, Macromolecules 52 (2019) 9585–9593.
[30] S.L. Anna, G.H. McKinley, J. Rheol. 45 (2001) 115–138.
[31] C. Clasen, J. Eggers, M.A. Fontelos, et al., J. Fluid Mech. 556 (2006) 283–308.
[32] A. Deblais, M.A. Herrada, J. Eggers, D. Bonn, J. Fluid Mech. 904 (2020) R2.